The response function of the Aragats Solar Neutron Telescope

A. Chilingarian, L. Melkumyan, G. Hovsepyan, A. Reymers*

Cosmic Ray Division, Alikhanyan Physics Institute, Alikhanyan Brovers 2, Yerevan AM-375036, Armenia

Abstract

The Aragats Solar Neutron Telescope (ASNT) is in operation at the Mt. Aragats research center (3200 m above sea level) in Armenia and constitutes part of the worldwide network, coordinated by Nagoya University. In this paper, we calculate the response function of the ASNT to the galactic and solar cosmic rays and determine the energy thresholds of the four ASNT channels. The capability of ASNT to distinguish the Ground Level Enhancements (GLEs) originated by solar neutrons is proposed and tested on the largest GLEs of the 23rd solar cycle.
© 2007 Elsevier B.V. All rights reserved.

PACS: 94.20.wg; 95.55.Vj; 24.10.Lx

Keywords: Solar cosmic rays; Particle detectors; Monte Carlo simulation

1. Introduction

The Sun influences the Earth in different ways by emission of radiation, plasma and high-energy protons, neutrons and ionized nuclei. Although the energy fraction carried by high-energy particles is very small compared with visible light energy, nonetheless, the study of these particles gives clues not only about fundamental and universal physical processes such as shock acceleration, but also provides timely information on the aftermath of the huge solar explosions affecting the near-earth environment and space borne and surface technologies, the so-called Space Weather issues [1].

Charged ions travel and reach the Earth by the "magnetic connection paths", between their birthplace and the Earth. The neutrons, originated from strong interactions on the Sun's surface, are not influenced by solar and interplanetary magnetic fields. They reach Earth directly from their place of birth on the solar disc. This feature allows us to "map" the solar accelerators location and provide the "time stamp" of the neutron production. To use this information, we need to detect the solar neutrons, distinguish them from solar protons and ions, estimate their energy, and determine their incoming direction. The first step to achieve these enhanced possibilities of neutron detection was to establish the network of Solar Neutron Telescopes (SNTs) [2], installed at seven locations on high mountains around the world, forming the second worldwide particle detector network, the Neutron Monitor (NM) [3] network being the first.

Acceleration of protons and ions on the Sun is associated with the reconnection of the intense magnetic fields on the Sun's surface. Moving along magnetic loops, ions reach the loop roots and interacting with dense solar plasma, give birth to copious particles including relativistic neutrons. In some circumstances, which are not completely understood yet, the flux of the solar neutrons is so intense that neutrons are detected by space-based and surface particle detectors [4]. If the magnetic loops opened due to ejected coronal plasma, the ions accelerated in the same episodes and moving along the magnetic lines connecting the Sun and Earth, also reach the Earth's magnetosphere. During violent explosions on the Sun, neutrons, protons and ions from Sun form additional flux Solar Cosmic Rays (SCR) to the generally existing Galactic Cosmic Ray (GCR) flux.

Approximately once per year, Solar Energetic Particles (SEP) have enough energy to penetrate the terrestrial

---

*Corresponding author.
  E-mail address: arthur@crdlx5.yerphi.am (A. Reymers).

atmosphere and generate cascades extended enough to reach the Earth's surface and be registered. These, very rare events, so-called Ground Level Enhancements (GLE) are well pronounced at high latitudes in polar regions; at middle latitudes, where the particle detectors of the Aragats Space Environmental Center (ASEC) [5] are located, the count rate enhancements are not large, usually 1–2 percents.

We use Monte Carlo simulation and calibration provided by the MAKET-ANI Extensive Air Shower (EAS) detector [6] to obtain important parameters of the Aragats Solar Neutron Telescope (ASNT) [7] and data analysis methodologies. The GEANT3 [8] and CORSIKA [9] simulation codes provide reliable platform for modeling the traversal of particles in the detector and atmosphere, respectively. We also perform a calibration experiment measuring fluxes of the EAS muons and electrons incident on the thick (60 cm) and thin (5 cm) scintillators of the ASNT for the validation of the simulation. For each four of the ASNT detecting channels, we determine the efficiency and purity of registered secondary particle fluxes. By analyzing the count rates of the ASNT channels, we estimate the minimal energy releases (energy thresholds) corresponding to four channels of the ASNT. A simple method for distinguishing the GLEs originated by solar neutrons is proposed and tested on the largest events of the 23rd solar cycle.

2. Aragats Solar Neutron Telescope

Starting from 1996, the group from the Solar-Terrestrial laboratory of Nagoya University has coordinated the world-wide network of SNTs located at seven longitudes uniformly distributed around the Earth. At least two neighboring detectors of this network can see the Sun disc simultaneously as the Earth makes its 24 h spin around its own axis [2].

The Aragats SNT is formed from four separate identical modules, as shown in Fig. 1. Each module consists of standard slabs of $50 \times 50 \times 5 \, cm^3$ plastic scintillators stacked vertically on a $100 \times 100 \times 10 \, cm^3$ horizontal plastic scintillator slab. Scintillator slabs are fine polished to provide good optical contact of the assembly. The slab assembly is covered by white paper from the sides and bottom and firmly kept together with special belts. Total thickness of the assembly is 60 cm. Four detectors of $100 \times 100 \times 5 \, cm^3$ size each located above the thick scintillator assembly as is seen in Fig. 1, are used to indicate charged particle traversal. This information is used
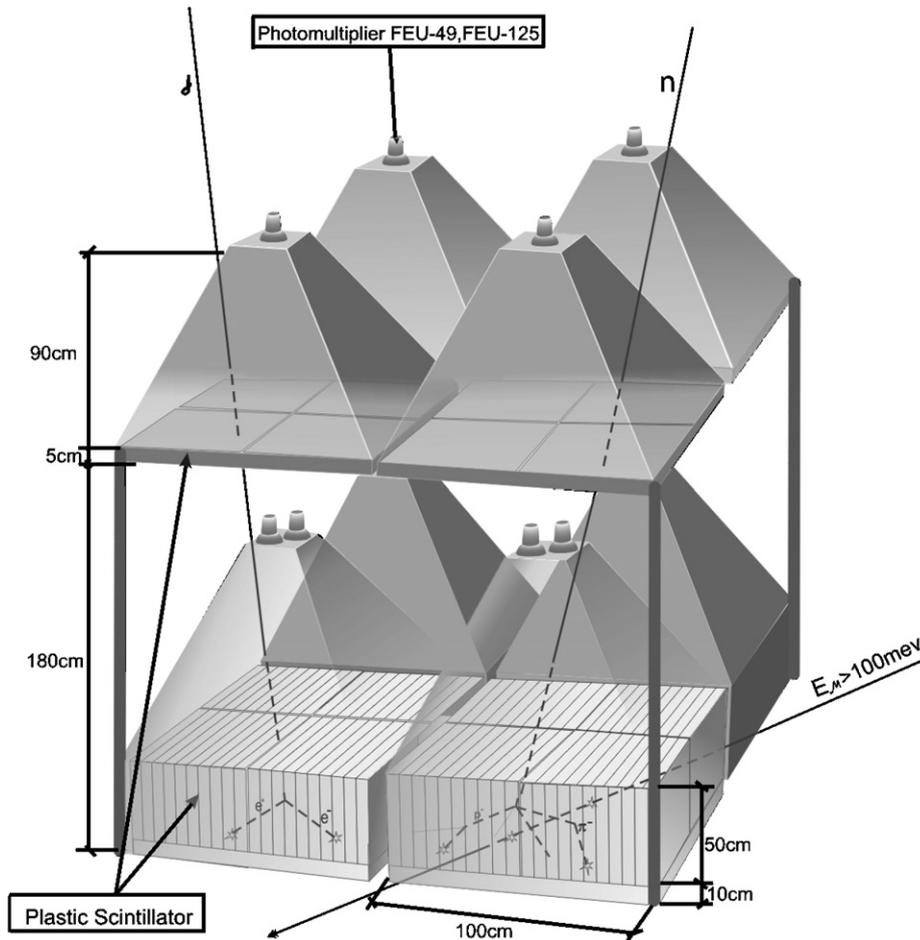

Fig. 1. Aragats Solar Neutron Telescope.

for selecting neutral particles and "vetoing" charged particles. A scintillator light capture cone and Photo Multiplier Tube (PMT) are located on the bottom and top assembly.

Incoming neutrons undergo nuclear reactions in the thick plastic target and produce protons and other charged particles. The intensity of the scintillation light induced by these charged particles has a dependence on the neutron energy and is measured by the PMT on the scintillators. To get information about the energy release in the scintillator, we discriminate each PMT output signal according to four predetermined threshold settings (50, 100, 150, 200 mV). Charged particles are very effectively registered both by the upper thin 5 cm and the lower thick 60 cm scintillators. When a neutral particle traverses the thin scintillator, typically no signal is produced. The absence of signal in the upper scintillators, coinciding with signal in the thick lower scintillators, points to neutral particle detection. In addition to the neutral signal, we will have many inclined traversals (not producing "veto" signal) of the charged particles. Therefore, the output information from ASNT is rather complicated. We perform detailed simulation of the detector response function to estimate the minimal energy releases corresponding to the PMT discrimination levels, to determine effectiveness of the charged particle "veto" and to quantify statements about detection of the different types of particles by the ASNT.

3. Monte Carlo simulation of ASNT response

We use the CORSIKA code [9] to simulate the cascade of *the secondary charged and neutral particles* up to the altitude of 3200 m, where the ASNT is located. The threshold energy for the primary charged particles used as input for CORSIKA corresponds to the rigidity cutoff of the location ~7.56 GV. All secondary particles were tracked till their energy dropped below a predetermined value (50 MeV for hadrons, 10 MeV for muons and 6 MeV for electrons). The spectra of primary protons and helium nuclei (99% of the flux at energies up to 100 GeV) are selected to follow the proton and helium spectra reported by CAPRICE98 balloon-borne experiment [10]. Among different species of secondary particles, generated in nuclear–electromagnetic cascades in the atmosphere, muons, electrons, γ-s, neutrons, protons, pions and kaons were followed with CORSIKA and stored. These particles were used as input for the GEANT3 package [8], the main platform for the detector response simulation. The secondary particles, their energies and angles of incidence obtained from the CORSIKA simulations allow us to develop a "particle generator" (distributions of the secondary particles on the top of the detector) used as input of the GEANT3 package.

For the estimation of light attenuation in the scintillator, we assume a simple model dividing the detector volume to 11 horizontal layers (see Fig. 2). The attenuation of the light intensity was calculated according to the absorp-
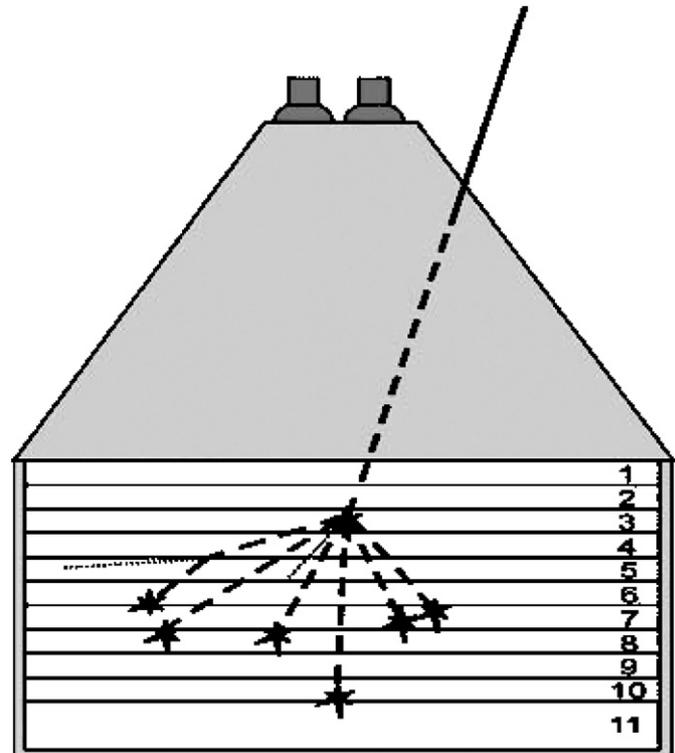

Fig. 2. The division of the thick scintillation detector into 11 layers.

Table 1
Fraction of light intensity reaching the PMT from each layer (in %)

Scintillator layers	Light output (%)
1	89.3
2	73.96
3	61.31
4	50.1
5	40.96
6	33.64
7	27.56
8	22.56
9	18.92
10	15.6
11	11.5

tion coefficients obtained from Ref. [11]. Fractions of light reaching the PMT from all 11 layers are depicted in Table 1.

To distinguish between total amount of energy released in scintillator and actual amount of energy registered by ASNT channels, we introduce notions of *genuine energy release* and *registered energy release*. Registered energy is proportional to the PMT output amplitude, and amplitude in turn is proportional to amount of light reaching photocathode of PMT. Thus, notion of the registered energy release include light attenuation in thick scintillator slab.

In simulations for each particle traversing the scintillator, we store both *genuine* and registered energy releases. In Figs. 3 and 4, we present distribution of the energy releases
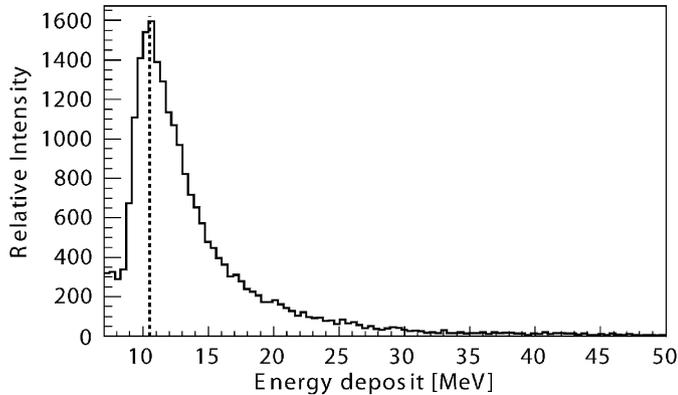
Fig. 3. Simulated energy release in the thin 5 cm upper scintillator of the SNT.
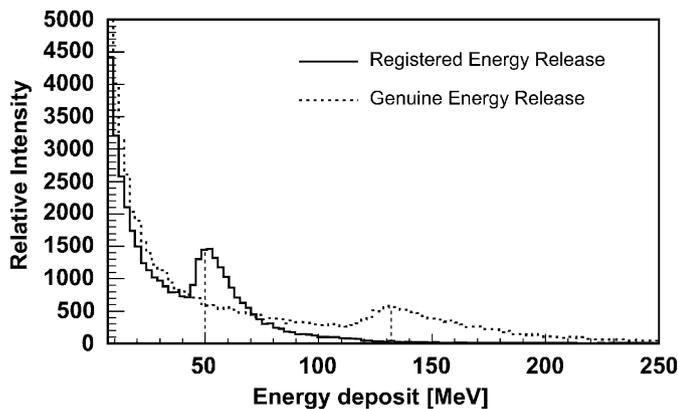

Fig. 4. Histogram of energy releases in 60 cm scintillator.

in thin and thick scintillators. In the 5 cm scintillator, the light attenuation did not affect the distribution shape and mode position (distribution mode equals ~10.5 MeV). In the thick scintillator, the position of the mode of the energy release distribution is shifted from ~50 MeV (*registered*) to ~130 MeV (*genuine*).

The rather broad peak in energy releases distribution of the thick scintillator (Fig. 4) is explained by the various paths of particles in the scintillator volume, thus allowing different energy releases. In the thin scintillator, the sharp peak is explained by the muons (constituting majority of the secondary particles at 3200 m) traversing the scintillator.

4. Estimation of the threshold energies of ASNT channels

Simulated distributions of the energy releases in thin and thick scintillators of ASNT should be compared with experimentally measured ones to prove the adequateness of the simulation and establish the relation between measurement units in the simulation and instrumentation. As we see in Figs. 3 and 4, from simulations we get energy releases in MeV scale, although the PMT output is in volts.

To perform the calibration of the PMT response, we used the registering channels of the MAKET-ANI surface

array [6] at the same location as the ASNT, equipped with the same type of scintillators. The MAKET-ANI surface array measures EAS, i.e., the secondary particles initiated in the terrestrial atmosphere by very high-energy protons and nucleus of the GCR flux. The density of charged secondary particles can reach tens of thousands per m^2, therefore, the logarithmic Analog-to-Digital Converters (ADC) are used to transform the PMT signal to a digital code and store on the online PC. The ADC is fabricated and tuned in such way that the ADC code K is proportional to the logarithm of the PMT signal amplitude:

$$K = \text{int}\{d \ln A_{\text{PMT}}\} + \text{constant}, \tag{1}$$

where A_{PMT} is the PMT signal amplitude and d is the scale factor, the so-called decrement. The ADC is precisely tuned with special electronics to keep the decrement value $d \sim 10$ within $\pm 2\%$. The "registering channel" assembly of MAKET-ANI array, which includes the PMT and the ADC, was mounted on the 60 cm thick scintillator housing and a histogram of the energy releases was obtained. The position of the distribution mode (peak) is dependent on the value of the high voltage applied to PMT. The PMT high voltage needs to be low enough so as not to amplify the PMT inherent noise, and high enough to maintain detector efficiency. The mode of the distribution of the PMT attached on the 5 cm thick detector was $K = 5$–6. This value is related to the so-called minimal ionization particle, "mip", traversing the thin 5 cm scintillator. As it is seen in Fig. 5, for the same "registering channel" attached on 60 cm thick detector, the distribution mode is shifted to code $K_{60} = 21$, therefore this code corresponds to the "mip" traversing the 60 cm thick scintillator.

This shift of the mode of the energy release distribution indicates that on average the amount of light reaching the photocathode of PMT from a mip traversing the thick 60 cm scintillator is 4.5 times larger, than the amount of light reaching the PMT from a mip traversing the 5 cm scintillator.

The ADC provides linearity in the code interval of $[0 < K < \sim 80]$, therefore, we can write

$$K_{60} - K_5 = d \ln \frac{A_{60}}{A_5}, \tag{2}$$

where $d = 10$ and the ratio of the amplitudes $A_{60}/A_5 = 4.5$.

We can conclude that the amount of light released in the 60 cm scintillator is also ~4.5 times more than in the 5 cm scintillator. Assuming that the most probable energy release in the 5 cm scintillator is equal to ~10.5 MeV [12,13], we conclude that the most probable energy deposited by a mip traversing the thick scintillator should be ~47 MeV. On the other hand, the average energy release from a single particle, under the condition of perfect transparency of the 60 cm thick scintillator, should be 12 times more than in the 5 cm thick scintillator, assuming the particle is energetic enough not to come to a stop in the scintillator. In other words, the PMT should measure 12
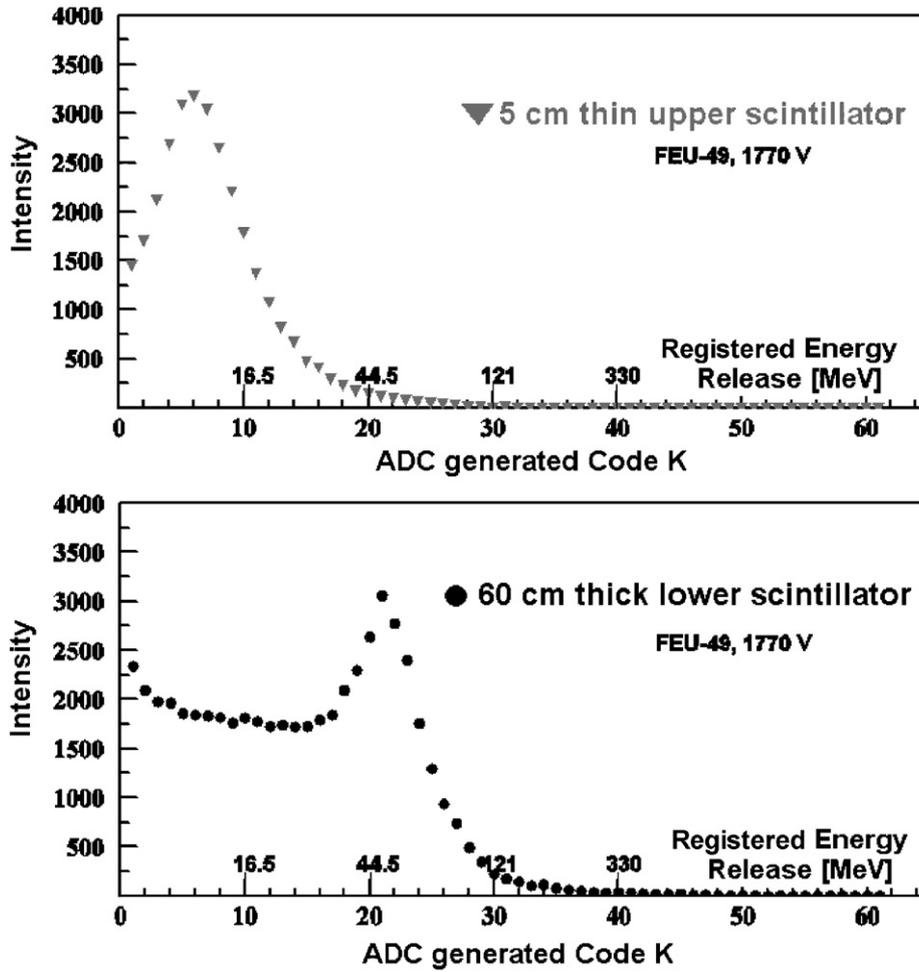
Fig. 5. Energy release spectra in 5 and 60 cm scintillators, using the same measuring channel with identical settings.

times more light intensity on the thick scintillator or the code K_{60} should be equal to 31, and not 21. This difference in the codes indicates that the light collection from the 60 cm thick scintillator is 2.7 times less than expected (a 10-point difference between codes corresponds to ratio of amplitudes of 2.7). Thus, if one takes into account absorption of light in the thick scintillator the most probable energy release should be $\sim 47 \times 2.7 \approx 127$ MeV. In this way, we find the relation between the two scales (codes and energy releases) using the position of the distribution (histogram) modes in 5 and 60 cm thick scintillators.

We obtain the distribution of the energy releases in thick scintillator in energy scale (MeV) without invoking results from GEANT simulation of the ASNT. We use only experimental result on the shifting of the mode of energy releases (PMT output in volts transformed to ADC codes) and independent measurement of the energy release in 5 cm thick scintillator (in MeV). Now we can compare obtained distributions with independent GEANT simulations. As we can see in Fig. 6, the two are in very good agreement proving relevance of our simulation and validity of the calibration procedure.

As well, after obtaining the appropriate scale for the measured distribution of the energy releases we can determine the energy thresholds corresponding to the four discrimination levels of the ASNT. We use experimentally measured intensities for each of the four ASNT channels ($M_i \sim 300$, 96, 28 and 11 counts/s). By numerically integrating the histograms of energy releases measured by ASNT, we can obtain the energy threshold corresponding to each channel:

$$M_i = \sum_{B_i}^{60} m_i, \tag{3}$$

where B_i is the threshold value of the ith channel of ASNT and m_i is the number of events fallen in the ith histogram channel (bin). We restrict summation with maximal bin corresponding to the code value 60, because the content of higher bins is vanishingly small. By summation of contents of the histogram bins from the selected one (low summation limit) up to the highest bin, we solve the system of Eq. (3) for all B_i, $i = 1$, 4 values. Fig. 7 illustrates the method. For example, to fit to the intensity $I = 300$ counts/s we started the summation of histogram channels from code $B_1 = 17$ (~ 32 MeV). Using the same scale factor of 2.7 we can obtain

the energy thresholds for the "genuine" energy releases. The results of the calculations for registered and genuine energy releases are summarized in Table 2. We add in Table 2, the
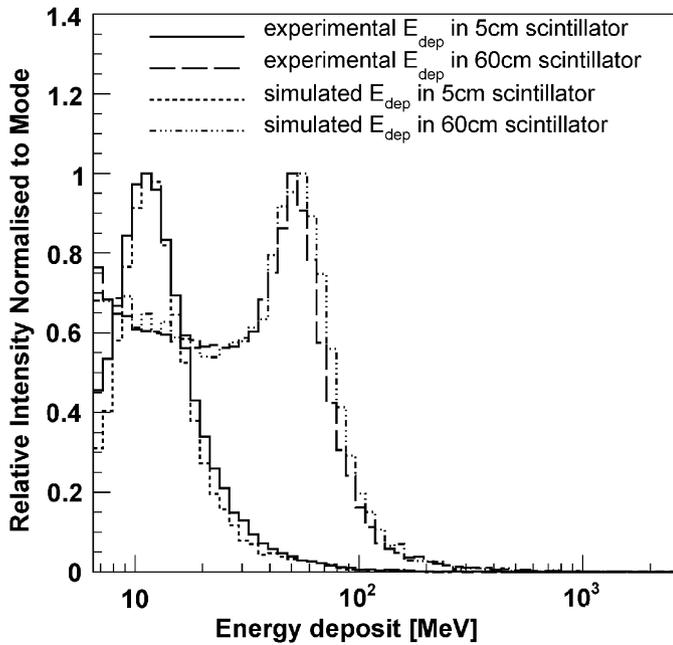
so-called 0 channel of ASNT, the count rate of detector without any discrimination of the output PMT signal. The count rate of 0 channel is rather large $M_0 = 690$, including all short traversals of 60 cm thick scintillator slab by inclined muons and electrons, as well as by γ-quanta conversing in scintillator to electron–positron pairs.

5. Efficiency of neutron registration and different particle fraction registered by ASNT channels

The efficiencies of registration of neutrons for all four thresholds are plotted in Fig. 8. As we can see from the figure, the first channel has efficiency $\sim$24% for the 300 MeV neutrons; the efficiency of the greater channels

Fig. 6. Comparison of modeled and measured energy releases in 5 and 60 cm scintillators.

Table 2
ASNT energy thresholds for registered and genuine energy releases of particles in the 60 cm scintillator

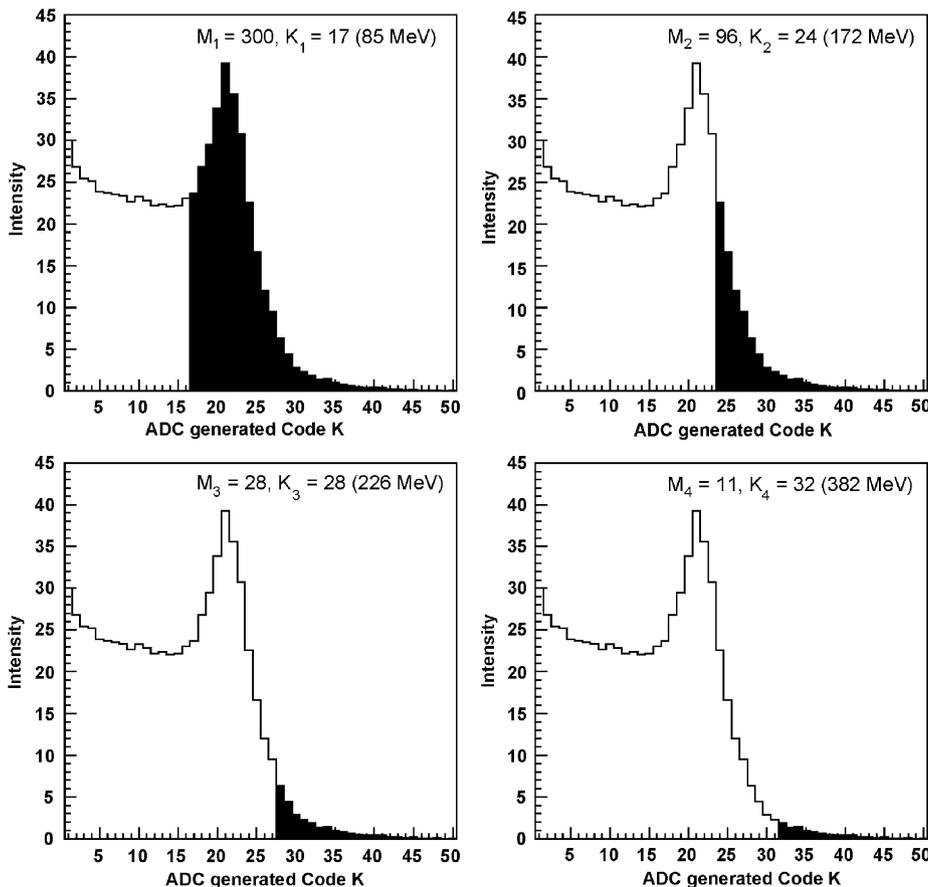| No. of ASNT channel	Intensity (count rate) (particles/s)	Threshold energy for registered energy release (MeV)	Threshold energy for genuine energy release (MeV)
0	690	6.4 ± 0.3	17.2 ± 0.9
1	300	32 ± 1.6	85 ± 4.3
2	96	64 ± 3.2	172 ± 8.6
3	28	95 ± 4.7	256 ± 12.8
4	11	141 ± 7.1	382 ± 19.1

Fig. 7. Illustration of the technique of obtaining the thresholds of SNT. The dashed regions correspond to ASNT intensities.

is much less. At the same neutron energies, the efficiency determined by the acceleration experiment for the Bolivian type SNT (same as at Aragats) by the Nagoya university group [14] is approximately 18%. The difference can be explained by the greater thickness of the Aragats SNT (60 cm) comparing with SNT used at Bolivian experiment (40 cm). Consequently, efficiencies of the other SNT channels are greater for the Aragats SNT. As was expected
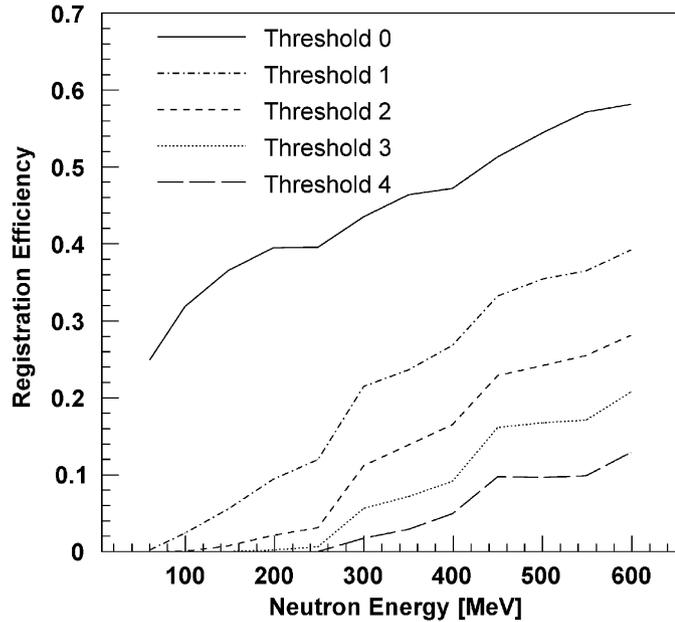

Fig. 8. Efficiency of registration of the neutron by different SNT channels depending on the neutron energy.

the efficiency of the 0 channel is very large, on the price of low purity, as we will see in Fig. 9.

Four channels of the ASNT "select" secondary particles in different proportions due to their different thresholds. If we assume that secondaries are generated by the GCRs only, the pattern of the particle proportions obtained from the simulations is depicted in Fig. 9.

In Fig. 9 and Table 3, these proportions are presented for the two cases: with and without "veto" on charged particles. The purity of the first ASNT channel to select neutrons is rather low, first channel "selects" mostly electrons and muons (80%), neutrons and protons only ~10% of registered particles; for the fourth channel, the situation is vice versa: electrons and muons ~30%, neutrons and protons ~60% of registered events. If we invoke the veto option, an enlarged fraction of neutral particles for all four ASNT channels is observed. This information is very important in treating the relative enhancements of SNT channels during the GLEs and other solar modulation effects. The zero channel registers copious low-energy electrons and γ-quanta adding to ASNT count rate.

6. Response of ASNT to the solar neutrons and protons

To estimate expected response of ASNT to SCR, we perform simulations of the particle traversal in the atmosphere using following fluxes of solar neutrons and protons, adopted from the GLEs registered during the 23rd solar cycle.
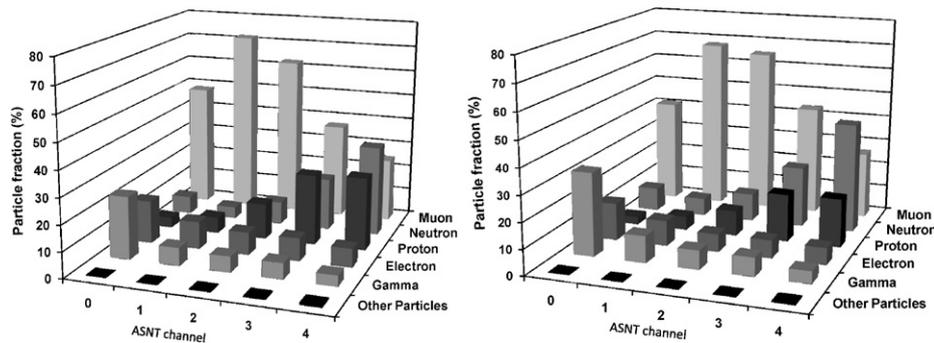

Fig. 9. "Purity" of selected events by the ASNT channels (on the left without veto, on the right with veto). Horizontal scale denotes the ASNT five channels, vertical particle proportion in percents.

Table 3
The fraction of different particles registered by the ASNT channels (in %)

No.	Other particles		Gamma		Electron		Proton		Neutron		Muon	
		Veto		Veto		Veto		Veto		Veto		Veto
0	0.07	0.04	24.22	32.47	16.59	14.56	3.92	2.94	6.86	9.19	48.34	40.80
1	0.10	0.07	6.95	10.45	10.57	9.84	6.19	5.29	4.51	6.84	71.68	67.52
2	0.21	0.10	6.11	7.38	8.69	6.93	13.81	9.81	8.75	10.86	62.43	64.93
3	0.37	0.16	6.19	7.26	8.85	6.94	27.31	18.61	20.25	23.74	37.03	43.30
4	0.64	0.43	4.17	4.74	7.22	6.47	28.25	18.97	34.99	43.10	24.72	26.29

The neutron spectrum from 100 MeV to 2 GeV at the top of the terrestrial atmosphere was adopted from Ref. [15] to be the following:

$$I_n(E) = 176E^{-3.6} (m^2 \text{ sterad s GeV})^{-1}. \quad (4)$$

Spectra of secondary particles from the neutron traversal in the terrestrial atmosphere were obtained by the PLANETOCOSMICS code [16]. Obtained secondary spectra well coincide with ones reported in Ref. [17].

The proton spectrum from 7.6 to 50 GeV was adopted from Refs. [18,19] as follows:

$$I_p(E) = 4.1 \times 10^5 E^{-5} (m^2 \text{ sterad GeV})^{-1}. \quad (5)$$

The secondary spectra were obtained in the same way as for the primary neutron flux and both spectra were used as input to GEANT3.

Obtained ASNT response to both types of solar particle fluxes is depicted in Table 4 (the 0 channel counts of thick scintillator). The enhancement of the 5 min count rate due to additional flux of the solar particles is shown in the units of "number of standard deviations" (relative errors). Relative standard deviations of thin and thick detectors were measured on a day when no disturbances took place and are equal to $\sigma_5 = 0.54\%$, $\sigma_{60} = 0.46\%$.

It is apparent from Table 4 that both proton and neutron GLEs will be detected unambiguously by ASNT. Furthermore, the neutron GLEs will be distinguished with very high reliability from proton GLEs. If we have large enhancement in the thick scintillator and much smaller enhancement in the thin scintillator, it points on the "neutron" GLE. This issue is very important, because until now, there has been no reliable method of distinguishing neutron GLEs by data from surface detectors [15].

The proposed technique was applied to the GLE detected by ASEC monitors due to events of the 23rd

Table 4
Simulated enhancement of the 5 min count rates (in numbers of standard deviations) due to fluxes (4) and (5)

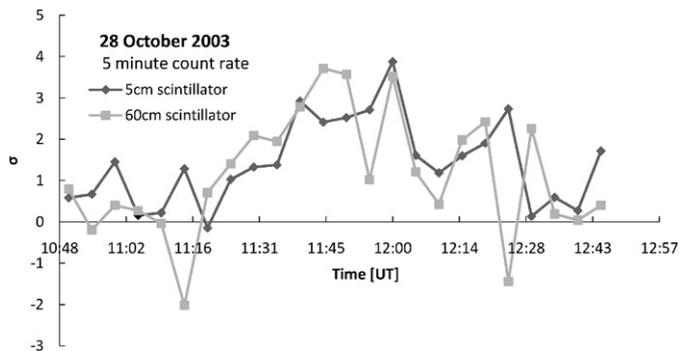|	Solar protons	Solar neutrons
5 cm scintillator	4.6σ	2.1σ
60 cm scintillator with veto	5.4σ	6.8σ

Fig. 10. GLE # 66 expressed in number of standard deviation measured by ASNT on October 28, 2003.
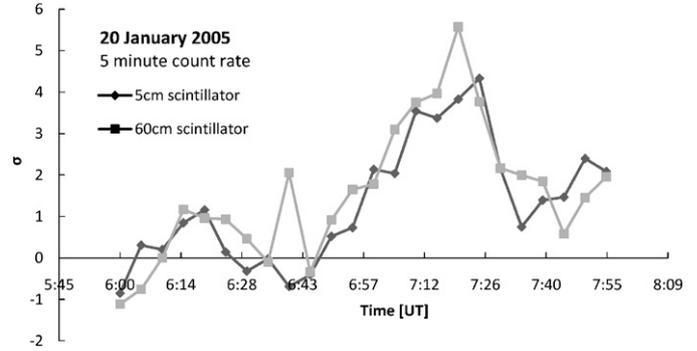

Fig. 11. GLE # 69 expressed in number of standard deviation measured by ASNT on January 20, 2005.

solar cycle. As we can see in Figs. 10 and 11, we have no evidence to claim that these GLEs were generated by solar neutrons. Both 5 and 60 cm detectors demonstrate the same enhancement, therefore we conclude that primary particles were solar protons.

7. Conclusion

We calculated the ASNT detector response function, including determination of the energy threshold of the detector channels, efficiency of the neutron detection by different channels, expected fraction of the various secondary particles detected by ASNT channels. We proposed a viable method of distinguishing GLEs initiated by the solar neutrons. By applying the proposed method to GLEs # 66 and # 69, we prove the proton nature of additional flux detected by the ASNT. Obtained characteristics of ASNT will be used for the further physical inference on solar extreme events detected in the years 2003–2005.

References

[1] J. Lilensten, J. Bornarel, Space Weather, Environment and Societies, Springer, Berlin, 2006.
[2] Y. Matsubara, Y. Muraki, et al., in: Proceedings of the 26th ICRC, Salt-Lake-City, 6, 42, 1999.
[3] H. Morall, A. Belov, J.M. Clem, Space Sci. Rev. 93 (2000) 285.
[4] E.L. Chupp, et al., Astrophys. J. 318 (1987) 913.
[5] A. Chilingarian, for the ASEC team, Nucl. Instr. and Meth. A 543 (2005) 483.
[6] V.V. Avakian, E.B. Bazarov, et al., VANT. Ser. Tech. Phys. Exp. 5 (31) (1986) 1.
[7] A.A. Chilingarian, et al., in: Proceedings of the 26th ICRC, Salt-Lake-City, vol. 1., 1999, p. 240.
[8] GEANT3.21—Detector Description and Simulation Tool, CERN Program Library Long Writeup W5013, CERN, 1993.

[9] D. Heck, et al., Forschungszentrum Karlsryhe, FZKA Report 6019, 1998.

[10] M. Boezio, et al., Astropart. Phys. 19 (2003) 583.

[11] J.A. Tsyrlin, Light-collection in scintillation counters, Atomizdat, 1975 (in Russian).

[12] Phys. Rev. D Particles and Fields, Part I, Review of Particle Physics, 2002, p. 84.

[13] E. Mnatsakanyan, et al., Calibration of the scintillation detectors of the particles density of the EAS. Preprint YerPhI 1610(8), 2006.

[14] H. Tsuchiya, et al., Nucl. Instr. and Meth. Phys. Res. A 463 (2001) 183.

[15] K. Watanabe, et al., Astrophys. J. 636 (2006) 1135.

[16] ⟨http://cosray.unibe.ch/~laurent/planetocosmics/⟩.

[17] S. Shibata, J. Geophys. Res. 99 (A4) (1994).

[18] M.Z. Zazyan, A.A. Chilingaryan, On the possibility to deduce proton energy spectrum of the 20 January 2005 GLE using Aragats and nor-amberd neutron monitors data, in: Proceedings of the 2nd International Symposium SEE-2005, Nor-Amberd, Armenia, 2005, pp. 200–202.

[19] ACE News #87—Feb 23, 2005. Space Weather Aspects of the January 20, 2005 Solar Energetic Particle Event, ⟨www.srl.caltech.edu/ACE/ACENews/ACENews87.html⟩.